This journal is © The Royal Society of Chemistry 2017

Computational details for calculating effective ionic radii

In order to obtain an effective ionic radius of a molecular cation, we first carried out geometry optimizations for finding the global energetic minimum on the potential energy surface (PES) in the gas phase. To sustain the best suited quantum mechanical level of theory for all following calculations, we performed geometry optimizations for the MA^+ cation substitutionary with restricted *Hartree-Fock* (RHF), second order *Møller-Plesset* perturbation theory (MP2), DFT, *coupled cluster theory* with single and double excitations (CCSD) and *coupled cluster* theory with single and double excitations with an additional estimate to triple excitations via perturbation theory (CCSD[T]). The basis set was chosen to be *split-valence triple* zeta with polarization functions, 6-311G**.

The bond lengths of the MA^+ cation vary to negligible amounts between all the investigated methods (< 1.6 % difference in total). The differences are less than 0.7 % for the C-N bond, < 1.1 % for C-H bonds

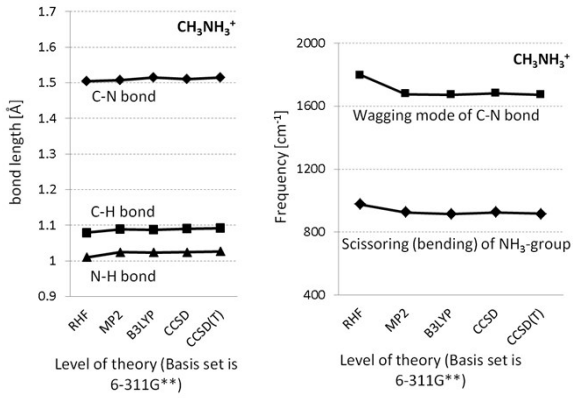

Fig. S1 left) Bond lengths of the MA^+ cation in the gas phase. The geometry depends on the quantum mechanical level of theory. For simple MA^+, the differences are less than 0.7 % (C-N bond), 1.1 % (C-H bond) and 1.6 % (N-H bond) for bond lengths among all investigated methods. **right)** Vibrational mode comparison. The difference in reciprocal wavelengths between the levels of theory is compared for the wagging mode of the C-N bond and the bending vibration of the amino-group. The C-N wagging differs less than 7.1 % and the NH_3 bending less than 6.5 % between the investigated methods.

and < 1.6 % for N-H bonds. The B3LYP functional reveals geometric values, which are closest to the gold-standard CCSD(T) results, with differences of less than 0.1 % for the C-N bond, 0.4 % for C-H bonds and 0.3 % for N-H bonds, respectively (Fig. 2, left). Vibrational frequencies reveal differences in reciprocal wavelengths of less than 7.1 % for the wagging of the C-N bond and less than 6.5 % for the bending modes of the NH_3 group. Again, the B3LYP functional shows values closest to the results from CCSD(T) method, with differences of less than 0.07 % for C-N wagging and < 0.34 % for NH_3 bending (Fig. 2, right). Accordingly, it is not necessary to use intense cpu-time requiring methods like CCSD or CCSD(T), since DFT with the B3LYP hybrid functional can be used instead.

In order to investigate the influence of the basis set on the final geometry in a more precise way, we performed DFT calculations on the MA^+ cation with several basis sets from mid-sized 6-311G** to large QZVP. As indicated in Fig. 3, the difference in total energy between the basis set 6-311G** and QZVP is negligible small (< 0.02 %), so it is reasonable and computationally more effective to use 6-311G**

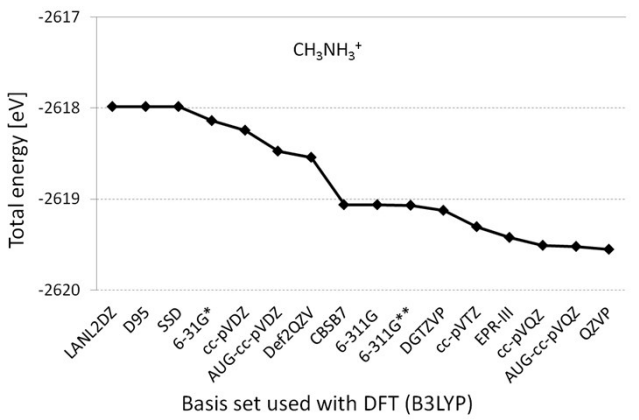

Fig. S2 Total energy of the MA^+ cation in the gas phase with respect to the basis set size used within the DFT (B3LYP) method. Large basis sets like cc-pVQZ or QZVP deliver the lowest energies, while the difference in total energy to the essentially less cpu-time requiring 6-311G is smaller than 0.02%.

basis set for further calculations (~ 340 times less cpu run-time requiring compared to QZVP). To account for closed shell systems, the spin-multiplicity *S* (*S* = 2s + 1) was fixed at 1. Furthermore, to check whether the optimized geometry is located on a minimum or on a transition state on the PES, we conducted frequency calculations based on the same level of theory and basis set (B3LYP with 6-311G** basis set). In the case where imaginary frequencies were found, bond lengths and angles of the hydrogen atoms involved in the corresponding thermal movement were changed until the optimization yielded only positive frequencies. In order to check whether the energetic minimum was a local or a global one, we performed conformational test calculations. The starting geometry of the molecule was changed by modifying the dihedral angles and the bond lengths of all involved atom-groups. In cases where three substantially different geometries resulted in the same optimized total energy, it was assumed that the global minimum was found. All calculations were carried out with the latest version of Gaussian electronic structure modelling software (Gaussian 09)[45]. The charge density treatment was conducted with the freely available molecule editor Avogadro[46,47].

We implied rotational freedom of the molecular cation around the center of mass in the optimized geometry. The total charge density was calculated first for NH_4^+ and the isocharge density was selected in a manner, that the radius of the sphere which contained the whole isocharge density in every possible orientation of the molecular cation, fits the literature reference value for its ionic radius[44]. Since molecular cations in hybrid ABX_3 compounds are located in a cuboctahedral void inside the BX_3^--framework, we chose the reference ionic radius in a 12-fold coordination (in $[NH_4]_2BX_6$) with an average of 1.695 Å. The resulting isocharge was found to be 0.013 electrons per cubic bohr [e^-/bohr^3]. The radii of the remaining 17 cations (Fig. 2) were calculated by applying the afore-mentioned isocharge density to the total electron density and by building a sphere which contained 100 % of this isocharge density in every possible orientation (for effective radii see Table S1, SI).

Table S1 Revised tolerance factors of 486 ABX_3 combinations for prediction of 3D perovskite formation

molecular cation	NH^{4+}	HY^{+}	HA^{+}	MA^{+}	FA^{+}	GUA^{+}	AZ^{+}	$DiMA^{+}$	EA^{+}	AA^{+}	$TetraMA^{+}$	IM^{+}	$TriMA^{+}$	$isoPA^{+}$	PY^{+}	$isoBuA^{+}$	$DiEA^{+}$	PhA^{+}
ionic radius [Å]	**1.70**	**2.20**	**2.26**	**2.38**	**2.77**	**2.80**	**2.84**	**2.96**	**2.99**	**3.00**	**3.01**	**3.03**	**3.04**	**3.07**	**3.22**	**3.60**	**3.85**	**3.88**
Cl^{-}																		
Ge^{2+}	0.972	1.110	1.126	1.159	1.266	1.274	1.285	1.318	1.327	1.329	1.332	1.337	1.340	1.348	1.390	1.494	1.562	1.570
Sn^{2+}	0.836	0.955	0.969	0.997	1.089	1.096	1.105	1.134	1.141	1.143	1.146	1.150	1.153	1.160	1.195	1.285	1.344	1.351
Pb^{2+}	0.883	1.008	1.023	1.053	1.150	1.158	1.168	1.198	1.205	1.208	1.210	1.215	1.218	1.225	1.262	1.357	1.419	1.427
Ca^{2+}	0.905	1.034	1.049	1.080	1.179	1.187	1.197	1.228	1.236	1.238	1.241	1.246	1.248	1.256	1.294	1.391	1.455	1.463
Sr^{2+}	0.833	0.951	0.966	0.994	1.085	1.092	1.102	1.130	1.137	1.139	1.142	1.146	1.149	1.156	1.191	1.280	1.339	1.346
Tm^{2+}	0.902	1.030	1.045	1.076	1.175	1.183	1.193	1.223	1.231	1.234	1.236	1.241	1.244	1.251	1.290	1.386	1.450	1.457
Sm^{2+}	0.873	0.998	1.013	1.042	1.138	1.146	1.156	1.185	1.192	1.195	1.197	1.202	1.205	1.212	1.249	1.343	1.404	1.412
Yb^{2+}	0.925	1.057	1.072	1.104	1.205	1.213	1.224	1.255	1.263	1.265	1.268	1.273	1.276	1.284	1.323	1.422	1.487	1.495
Dy^{2+}	0.858	0.981	0.995	1.024	1.119	1.126	1.136	1.165	1.172	1.174	1.177	1.182	1.184	1.191	1.228	1.320	1.380	1.388
Br^{-}																		
Ge^{2+}	0.961	1.094	1.109	1.141	1.243	1.251	1.262	1.293	1.301	1.304	1.306	1.312	1.314	1.322	1.362	1.462	1.527	1.535
Sn^{2+}	0.831	0.946	0.959	0.987	1.075	1.082	1.091	1.119	1.125	1.128	1.130	1.135	1.137	1.144	1.178	1.264	1.321	1.328
Pb^{2+}	0.879	1.001	1.015	1.044	1.138	1.145	1.154	1.183	1.191	1.193	1.195	1.200	1.203	1.210	1.246	1.337	1.397	1.405
Ca^{2+}	0.901	1.025	1.040	1.069	1.165	1.173	1.183	1.212	1.220	1.222	1.225	1.229	1.232	1.239	1.276	1.370	1.431	1.439
Sr^{2+}	0.828	0.943	0.956	0.984	1.072	1.079	1.088	1.115	1.122	1.124	1.126	1.131	1.133	1.140	1.174	1.260	1.317	1.324
Tm^{2+}	0.894	1.018	1.033	1.062	1.157	1.165	1.174	1.204	1.211	1.214	1.216	1.221	1.223	1.231	1.267	1.360	1.422	1.429
Sm^{2+}	0.916	1.043	1.058	1.088	1.186	1.194	1.204	1.234	1.241	1.244	1.246	1.251	1.254	1.261	1.299	1.394	1.457	1.464
Yb^{2+}	0.910	1.036	1.051	1.081	1.178	1.185	1.195	1.225	1.232	1.235	1.237	1.242	1.245	1.252	1.290	1.384	1.447	1.454
Dy^{2+}	0.870	0.990	1.005	1.033	1.126	1.133	1.143	1.171	1.179	1.181	1.183	1.188	1.190	1.198	1.233	1.324	1.383	1.390
I^{-}																		
Ge^{2+}	0.927	1.048	1.062	1.090	1.183	1.190	1.200	1.229	1.236	1.238	1.240	1.245	1.248	1.255	1.290	1.381	1.440	1.448
Sn^{2+}	0.869	0.981	0.995	1.022	1.109	1.115	1.124	1.151	1.158	1.160	1.162	1.167	1.169	1.176	1.209	1.294	1.350	1.356
Pb^{2+}	0.853	0.963	0.976	1.003	1.088	1.095	1.103	1.130	1.136	1.138	1.141	1.145	1.147	1.154	1.187	1.270	1.324	1.331
Ca^{2+}	0.883	0.997	1.011	1.038	1.126	1.133	1.142	1.169	1.176	1.179	1.181	1.185	1.188	1.194	1.228	1.314	1.371	1.378
Sr^{2+}	0.815	0.920	0.933	0.958	1.040	1.046	1.054	1.079	1.086	1.088	1.090	1.094	1.096	1.103	1.134	1.213	1.266	1.272
Tm^{2+}	0.874	0.988	1.001	1.028	1.116	1.122	1.131	1.158	1.165	1.167	1.170	1.174	1.176	1.183	1.217	1.302	1.358	1.365
Sm^{2+}	0.832	0.940	0.953	0.978	1.062	1.068	1.077	1.102	1.109	1.111	1.113	1.117	1.119	1.126	1.158	1.239	1.292	1.299
Yb^{2+}	0.880	0.994	1.008	1.035	1.123	1.130	1.139	1.166	1.172	1.175	1.177	1.182	1.184	1.191	1.224	1.310	1.367	1.374
Dy^{2+}	0.869	0.981	0.995	1.022	1.109	1.115	1.124	1.151	1.158	1.160	1.162	1.167	1.169	1.176	1.209	1.294	1.350	1.356

Table S2 Revised octahedral factors of 27 BX_3^- permutation.

Cl^-	octahedral factor μ
Ge^{2+}	0.395
Sn^{2+}	0.622
Pb^{2+}	0.535
Ca^{2+}	0.497
Sr^{2+}	0.627
Tm^{2+}	0.503
Sm^{2+}	0.551
Yb^{2+}	0.465
Dy^{2+}	0.578
Br^-	
Ge^{2+}	0.372
Sn^{2+}	0.587
Pb^{2+}	0.500
Ca^{2+}	0.464
Sr^{2+}	0.592
Tm^{2+}	0.474
Sm^{2+}	0.439
Yb^{2+}	0.449
Dy^{2+}	0.515
I^-	
Ge^{2+}	0.350
Sn^{2+}	0.441
Pb^{2+}	0.468
Ca^{2+}	0.418
Sr^{2+}	0.536
Tm^{2+}	0.432
Sm^{2+}	0.505
Yb^{2+}	0.423
Dy^{2+}	0.441

Table S3 Revised B^{2+} metal cation radii from Ref. 50 (Shannon radii used when colored in light blue!)

Shannon radius → X.XX

$r(M^{2+})$ revised	Cl^-	Br^-	I^-
Ge^{2+}	0.73	0.73	0.77
Sn^{2+}	1.15	1.15	0.97
Pb^{2+}	0.99	0.98	1.03
Ca^{2+}	0.92	0.91	0.92
Sr^{2+}	1.16	1.16	1.18
Tm^{2+}	0.93	0.93	0.95
Sm^{2+}	1.02	0.86	1.11
Yb^{2+}	0.86	0.88	0.93
Dy^{2+}	1.07	1.01	0.97

Table S4 Experimental radii of the three investigated halide anions

	***r*(X$^-$) experimental**
***r*(Cl$^-$)**	1.85
***r*(Br$^-$)**	1.96
***r*(I$^-$)**	2.20

Table S5 Proposed 106 ABX_3 combinations showing appropriate tolerance factors (0.9 < *TF* < 1.12) and octahedral factors (μ > 0.414) to allow for 3D perovskite formation. $AZSnI_3$ and $AZDyI_3$ exceed the *TF*-range but are geometrically considered to allow the formation of three-dimensional perovskite bulk phases.

Compound	*TF*	Compound	*TF*
HYSrCl3	0.951	DiMASmI3	1.102
HASrCl3	0.966	EASmI3	1.109
MASrCl3	0.994	AASmI3	1.111
FASrCl3	1.085	TetraMASmI3	1.113
GUASrCl3	1.092	IMSmI3	1.117
AZSrCl3	1.102	TriMASmI3	1.119
HYSnCl3	0.955	NH4TmCl3	0.902
HASnCl3	0.969	HYTmCl3	1.030
FASnCl3	1.089	HATmCl3	1.045
AZSnCl3	1.105	MATmCl3	1.076
HYSrBr3	0.943	HAPbBr3	1.015
HASrBr3	0.956	HYCaCl3	1.034
MASrBr3	0.984	HACaCl3	1.049
FASrBr3	1.071	MACaCl3	1.080
GUASrBr3	1.079	HYTmBr3	1.018
AZSrBr3	1.088	HATmBr3	1.033
DiMASrBr3	1.115	MATmBr3	1.062
HYSnBr3	0.946	AZPbI3	1.103
HASnBr3	0.959	NH4YbCl3	0.925
FASnBr3	1.075	HYYbCl3	1.057
GUASnBr3	1.082	HAYbCl3	1.072
AZSnBr3	1.091	MAYbCl3	1.104
DiMASnBr3	1.119	NH4CaBr3	0.900
HYDyCl3	0.981	HYCaBr3	1.025
HADyCl3	0.995	HACaBr3	1.040
MADyCl3	1.024	MACaBr3	1.069
FADyCl3	1.119	NH4YbBr3	0.910
HYSmCl3	0.998	HYYbBr3	1.036
HASmCl3	1.013	HAYbBr3	1.051
MASmCl3	1.042	MAYbBr3	1.081
HYSrI3	0.920	HYDyI3	0.981
HASrI3	0.933	HADyI3	0.995
FASrI3	1.040	MADyI3	1.022
GUASrI3	1.046	FADyI3	1.109
AZSrI3	1.054	GUADyI3	1.115
DiMASrI3	1.080	NH4SmBr3	0.916
EASrI3	1.086	HYSmBr3	1.043
AASrI3	1.088	HASmBr3	1.058
TetraMASrI3	1.090	MASmBr3	1.088
IMSrI3	1.094	HYTmI3	0.988
TriMASrI3	1.096	HATmI3	1.001
isoPASrI3	1.103	MATmI3	1.028
HYPbCl3	1.008	FATmI3	1.116
HAPbCl3	1.023	HYYbI3	0.994
HYDyBr3	0.990	HAYbI3	1.008
HADyBr3	1.005	MAYbI3	1.035

MADyBr3	1.033	HYCaI3	0.997
HYSmI3	0.940	HACaI3	1.011
HASmI3	0.953	HYSnI3	0.981
MASmI3	0.978	HASnI3	0.995
FASmI3	1.062	GUASnI3	1.115
GUASmI3	1.068	AZSnI3	1.124
AZSmI3	1.077	AZDyI3	1.124